High-resolution QEU maps for ACIS-I and S1,2,3 chips

A. Vikhlinin

Abstract

ECS data accumulated over several years of ACIS operations show the small-scale variations of the ACIS quantum efficiency — intra-node variations in the FI CCDs and strong column-to-column fluctuations in the BI chips. We report on creation of new high-resolution quantum efficiency non-uniformity maps (QEU) for ACIS-I and 3 CCDs in ACIS-S (S1, S2, and S3). This new calibration reduces the QEU uncertainties to 1%–2% from the present 5%.

1   Introduction

Between February, 2000 and the summer of 2003, ACIS has been exposed to the ECS for over 2.5 million seconds. The high statistical accuracy of the combined dataset allows one to study small-scale spatial variations in the ACIS quantum efficiency. Indeed, strong column-to-column variations for the BI chips are easily revealed (Fig. 1). These structures are not accounted for by the present calibrations, and indeed, could not be revealed in the data available in 2000 because of the limited statistics. The scope of the present work is 1) to develop the QEU maps with higher spatial resolution, and 2) improve the model for the energy dependence of the QEU correction. Our goal is to drive the QEU uncertainties down to a 1% level.

2   Calibration data and related analyses

We use the combined ECS dataset collected over February, 2000 – July, 2003 at the focal plane temperature -120 C. The data in the FI CCDs (we use all 4 of the ACIS-I chips and S2) were CTI-corrected. The time-dependent gain correction (***REF***) has been applied. Finally, we applied new gain tables matching the CALCRMF2 ACIS response calibration (***REF***); this is important only for S1.

The QEU analysis is based on the data for the three brightest emission lines in the ECS spectrum, Al-Ka at 1.487 keV, Ti-Ka+b at 4.510 and 4.93 keV, and Mn Ka+b at 5.898 and 6.486 keV. The chip images were extracted in the PI channel ranges 70–118, 3000-365, and 380–480 for the Al, Ti, and Mn lines, respectively. Note the for the Ti and Mn lines, our energy bands include both Ka and Kb lines (see the memo on the analysis of the Ball data). The ECS illumination pattern which must be taken into account in the QEU analysis was derived in the same memo.

3   Can the QEU signal be enhanced?

The QEU corrections are relatively small. For example, the intensity variations shown in Fig. 1 do not exceed 35% at Mn, and 12% at Al. It is therefore very difficult to measurements these variations sufficiently accurately in order to establish the QEU energy dependence and therefore to interpolate the corrections between 1.5 and 6 keV and to extrapolate them to lower and higher energies. *To study the QEU "signal" in detail, it must be enhanced.* We show below that this is indeed possible by splitting the photons into the appropriate ACIS flight grade groups.

The primary reason for the quantum efficiency variation is the event grade migration caused by the charge transfer inefficiency (CTI). A fraction of the charge is transfered into trailing pixels which can alter the photon grade from "good" to "bad". Most of the events with the "bad" grades correspond to the tracks of charge particles and therefore are sorted out both on orbit and during the Lev2 data processing.

Fig. 1— Image of the S3 chip in the Mn line. The image was blocked by a factor of 16 along the CHIPY direction to emphasize the column-to-column variations
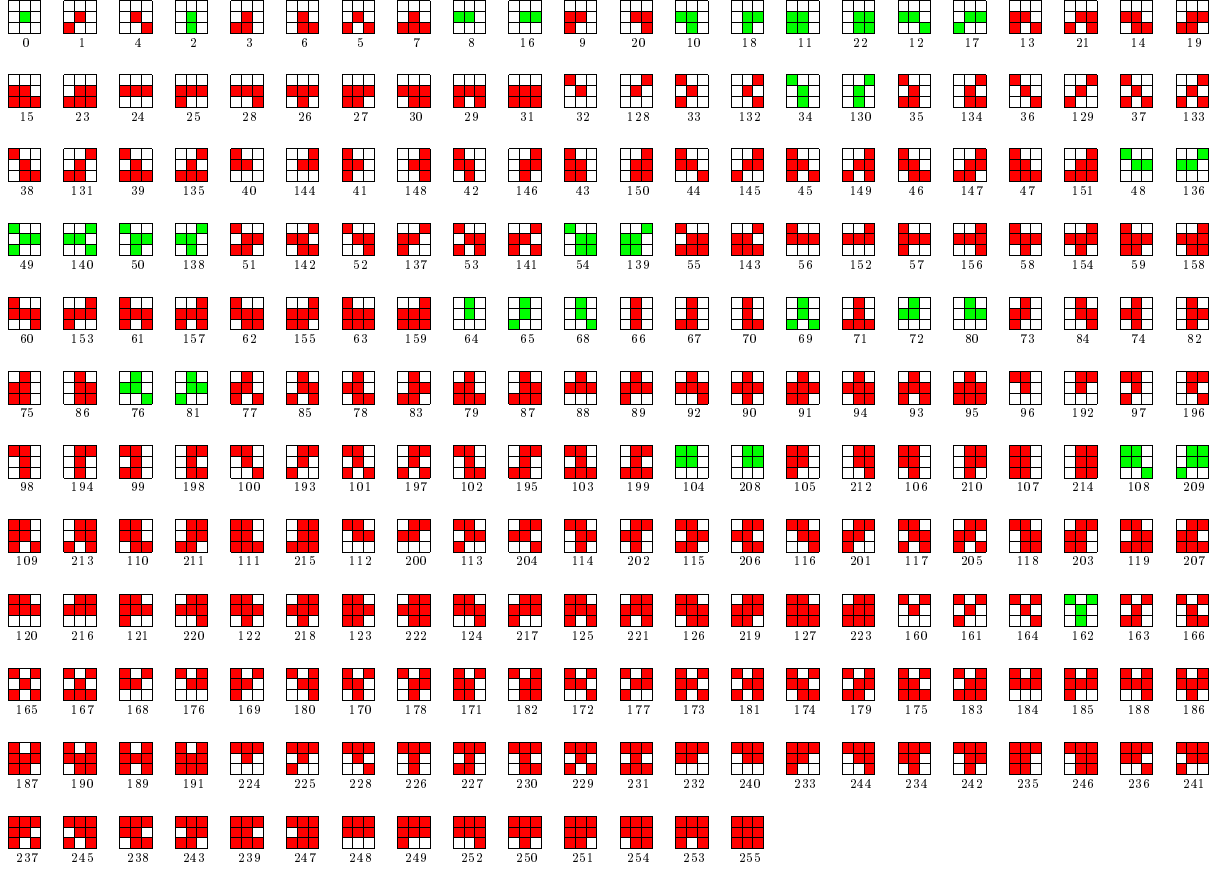
Fig. 2— ACIS grade patterns. The "good" grades are shown in green. The events with grades 0, 8, 16, 64, 72, 80, 104, 208 are not altered or migrate into each other if the charge is added to the trailing pixels; this is a "good good" (GG) set. Events with grades 2, 10, 18, 11, and 22 migrate into the "bad" grades because of the CTI; this is a "bad good" (BG) set. Other "good" grades (12, 17, 34, 130, 48, 136, 49, 140, 50, 138, 54, 139, 65, 68, 69, 76, 81, 108, 209, and 162) contain a negligible fraction (< 0.5%) of the total flux.

The definition of the ACIS event grades is reproduced in Fig. 2. The "good" grades are shown in green. The good grades can be split into two main groups. Events with grades 0, 8, 16, 64, 72, 80, 104, 208 are not altered or migrate into each other if the charge is added to the trailing pixels. We call this a "good good" (GG) set. On the contrary, events with grades 2, 10, 18, 11, and 22 easily migrate into "bad" grades because of the CTI; we refer to this as a "bad good" (BG) set. Other good grades (12, 17, 34, 130, 48, 136, 49, 140, 50, 138, 54, 139, 65, 68, 69, 76, 81, 108, 209, and 162) contain less then 0.5% of the total flux combined, and we discard them from the further analysis.

If the CTI is indeed the main reason for the quantum efficiency non-uniformities, *we expect that the QEU variations are almost absent in the GG set and much enhanced in the BG set.* The images of the S3 and S2 chips in the BG and GG grade sets dramatically confirm this expectation (Fig. 3, 4). This suggests the the accurate QEU model can be developed with the following approach:

1. Derive QEU (both spatial and energy dependence) for the BG set, $QEU_{BG}(X, Y, E)$.
2. Derive the fraction, f_{BG}, of the total flux in the BG set as a function of energy near the CCD readout where the QEU effects are small.
3. The final QEU model is obtained as

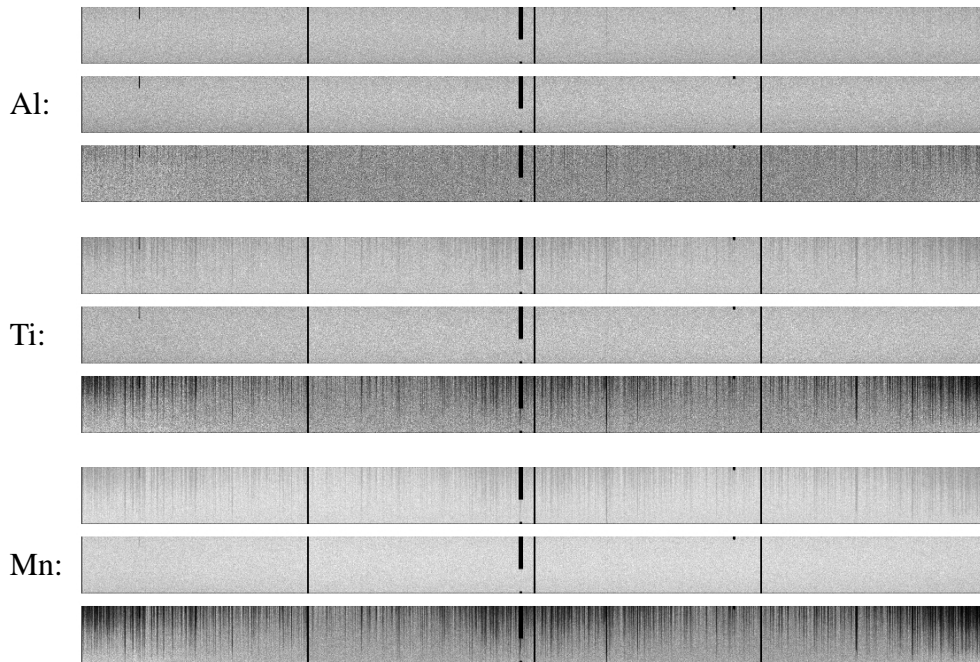$$QEU(X, Y, E) = 1 + f_{BG}(E) \times (QEU_{BG}(X, Y, E) - 1) \tag{1}$$

Fig. 3— S3 images in the Al, Ti, and Mn lines in the three grade sets — all, GG, and BG (top to bottom in each panel). As in Fig. 1, the images have a 1 pix resolution in the X direction and are blocked by a factor of 16 in the Y-direction. A slight decrease in intensity at the bottom of the CCD visible in the Al and Mn GG images is caused by the ECS illumination pattern.
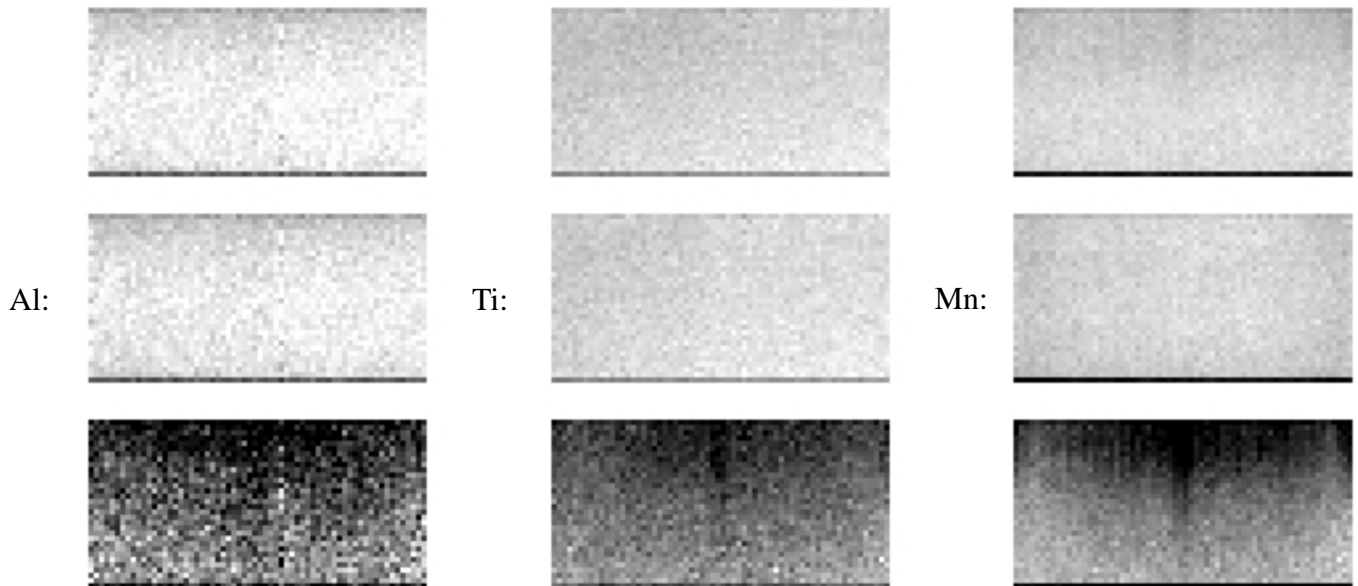

Fig. 4— Same as Fig. 3 but for the S2 chip. The images are blocked by a factor of 4 in the X-direction and by a factor of 32 in the Y-direction. Note that the QEU variations in the FI CCDs at $T = -120\,\mathrm{C}$ are small and become easily detectable only in the BG set.
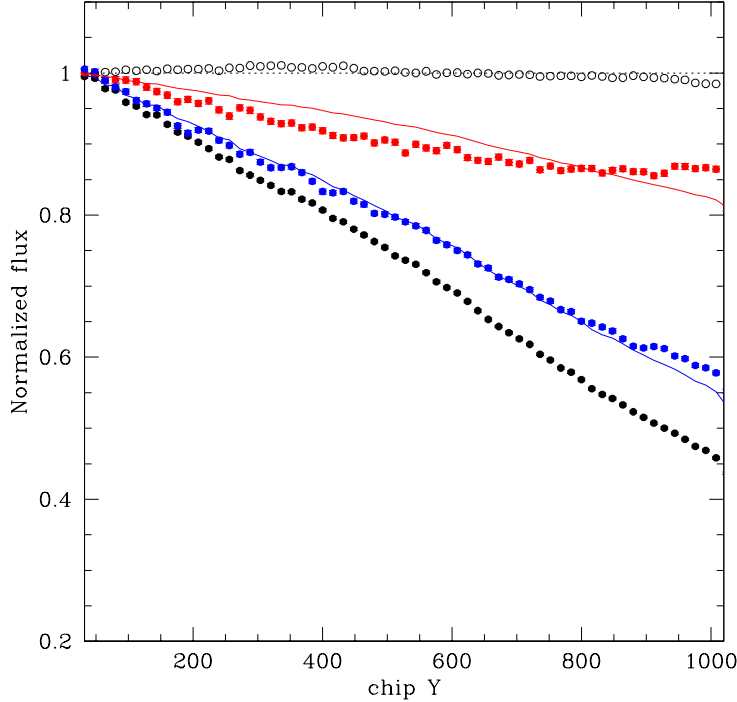
3

Fig. 5— Projection of the S3 images in the Mn, Ti, and Al lines (black, blue, and red, respectively) along the `CHIPX` axis. For Mn, both the ɢɢ (open circles) and ʙɢ (filled circle) projections are shown. For Ti and Al, we show only the ʙɢ data. The ECS illumination pattern has been corrected in all cases. The solid blue and red lines show the scalings of the Mn profile to Ti and Al assuming that the flux loss is $\log f \propto E$.

4 QEU for BI chips

Below, we provide a detailed report on the derivation of the QEU calibration for the S3 chip. A similar analysis is used for the S1 chip; the differences are outlined in §4.5.

4.1 Energy dependence: $\mathbf{QEU_{BG}}(E)$

The general idea about the energy dependence of the ʙɢ QEU can be obtained from projection of the ʙɢ images along the `CHIPX` axis (Fig. 5). The flux loss is clearly smaller towards lower energies. The following scaling provides an adequate description of the data

$$\log(f) \propto E, \tag{2}$$

where f is the observed intensity normalized to 1 near the CCD readout. The Mn projection scaled according to eq. (2) to 1.487 and 4.510 keV is shown in Fig. 5 by the red and blue lines, respectively. The agreement of the scaled profile is especially good for the Ti data. Note also that the ɢɢ projection for the Mn lines (open circles in Fig. 5) is constant within ±1%, within the measurement accuracy for the illumination pattern.

Additional tests for the energy dependence of the QEU can be made using the XRCF calibration. The S3 chip was uniformly illuminated by several monochromatic sources with in the 0.5–8 keV energy range. The ʙɢ and ɢɢ profiles from these measurements are shown in Fig. 6. At $E = 2.116$ keV and above, there is an excellent agreement with the in-flight Mn profile scaled as in (2). Below this energy (***ᴘʀᴏʙᴀʙʟʏ, ʙᴇʟᴏᴡ ᴛʜᴇ SɪK ᴇᴅɢᴇ ᴀᴛ 1.837 ᴋᴇV***), there are increasingly strong deviations from the scaling. In fact, *the data are more consistent with the energy-independent correction for* ʙɢ *events for $E < 1.837$ keV*. However, even if this is neglected, the error in the final QEU is small. For example, the deviations for the ʙɢ events at $E = 0.525$ keV are approximately 9%; the fraction of such events in the total flux is 12%–14% (see §4.3); therefore the error in the final QEU is 1.1%–1.2%. At Al there are 3% residuals, while the fraction of the ʙɢ events at 1.487 keV is $\lesssim 20\%$, therefore such residuals result in less than 1% inaccuracies of the final QEU calibration. This is a good example of why splitting the photons into ʙɢ and ɢɢ events helps to greatly improve the QEU calibration accuracy.
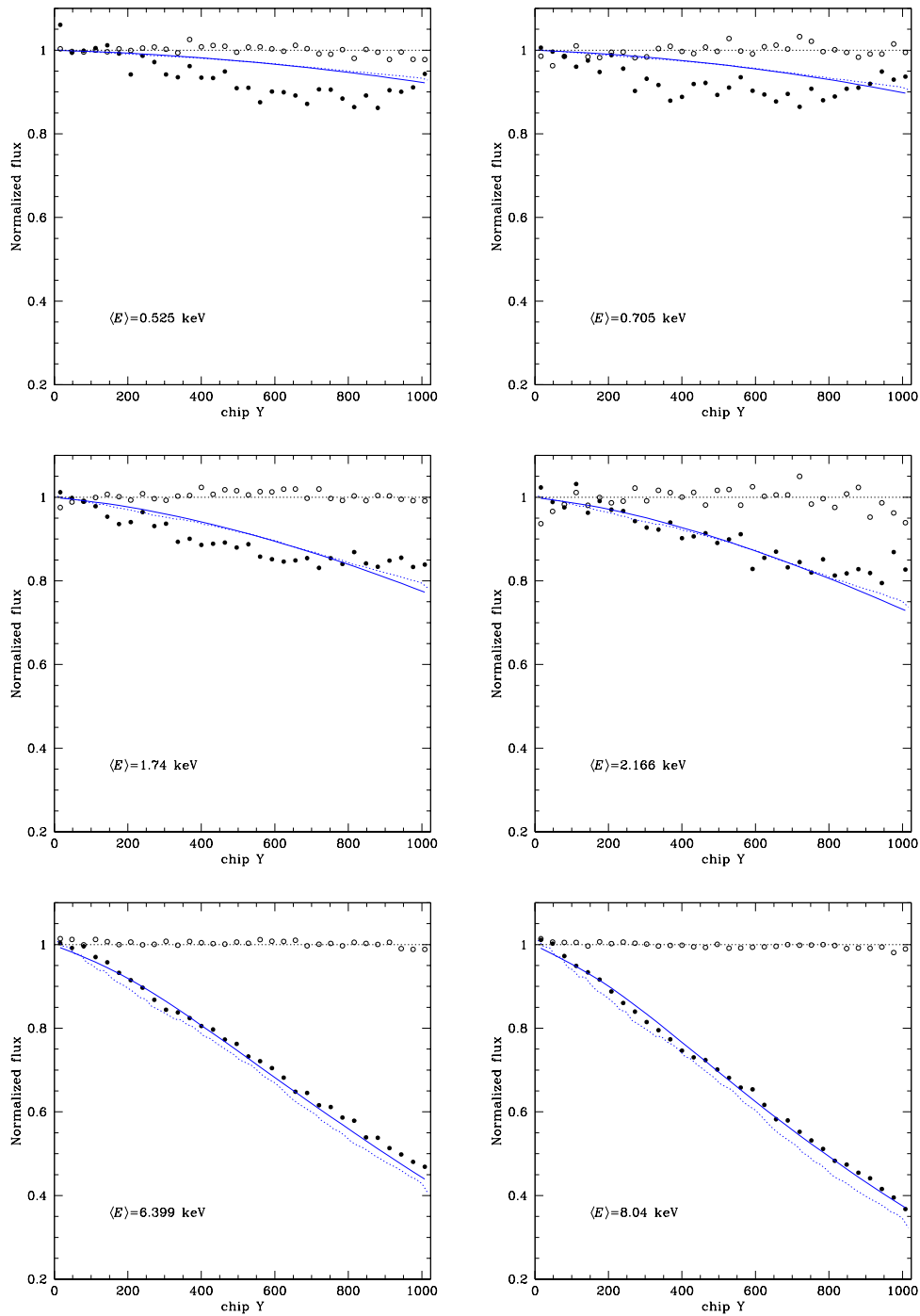
Fig. 6— Projection of the S3 images from the Phase-I calibration at the XRCF. Each plot shows projections for ʙɢ and ɢɢ events (filled and open circles, respectively). The blue lines show correction for the ʙɢ fluxes expected from the inflight Mn data (Fig. 5). The dotted line is the Mn pofile from Fig. 5 scaled by eq. (2); the solid line is the projection of the scaled correction map (see §4.4).
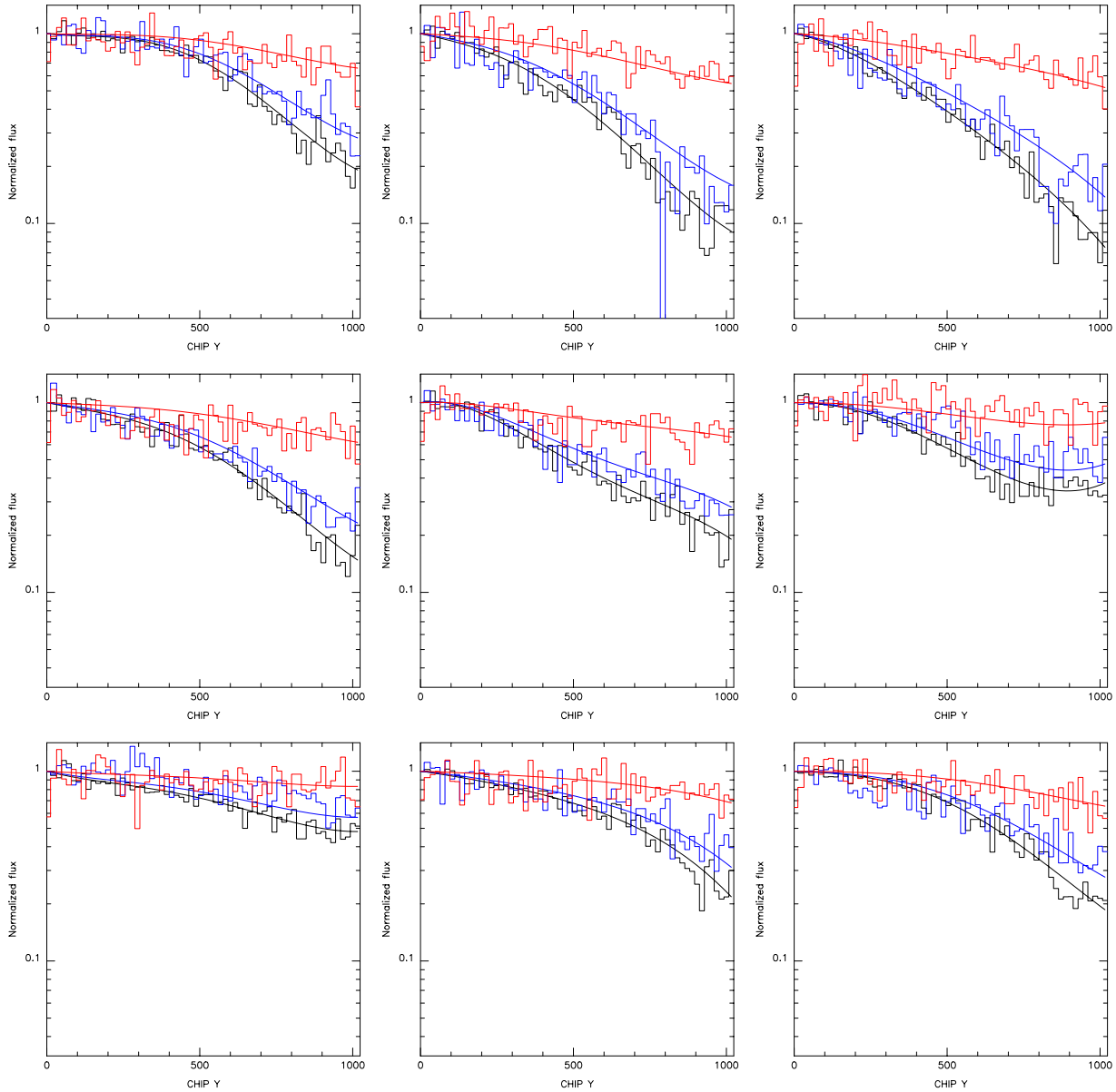
5

Fig. 7— Fits to the Mn ʙɢ data in the 9 consecutive CCD columns in S3 (CHIPX = 970 − 979). The Mn, Ti, and Al data are shown by black, blue, and red histograms, respectively. The 4-th order polynomial fit is to the Mn data only (black line); it is scaled using eq. (2) to Ti and Al (blue and red lines, respectively).

It has been verified that eq. (2) also describes the scaling of the flux loss for the individual CCD columns (see Fig. 7 below). Therefore, we will use this relation for the QEU energy dependence in the BI CCDs. ***Aɴʏ ᴘʜʏsɪᴄᴀʟ ᴇxᴘʟᴀɴᴀᴛɪᴏɴ ꜰᴏʀ ᴛʜɪs sᴄᴀʟɪɴɢ?***

4.2   Spatial dependence: $QEU_{BG}(X, Y)$ for Mn

Results of §4.1 suggest that the QEU calibration at Mn can be reliably scaled to other energies using eq. (2). The Mn line is the brightest in the ECS spectrum and has the strongest QEU signal. Therefore, the QEU at Mn can be easily calibrated with a high spatial resolution — in fact, on the column-by-column basis.

We use the following procedure:
1. The ʙɢ intensity profile is extracted in each CCD column for the Al, Ti, and Mn lines.
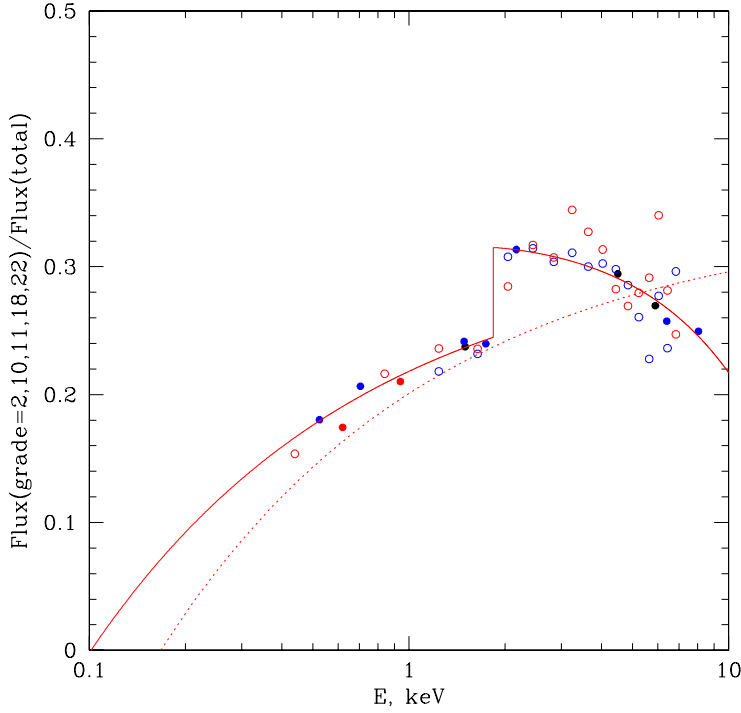
Fig. 8— The fraction of the BG events in the total flux as a function of energy. The data are for ECS and XRCF (black and blue filled circles), E0102 (red circles), and G21.5 and A1795 (open blue and red circles). The solid line shows the fit from eq. (3). The dotted line is from the *04/02/04* version.

2. The profiles are "flat-fielded" using the ECS illumination pattern and blocked into bins of 16 CCD pixels each.
3. The profiles are normalized to 1 near the readout by dividing by the average intensity in the `CHIPY` range 16–96.
4. Logarithm of intensity as a function of `CHIPY` is fit to the Chebyshev polynomials of the 4-th order. The fit is restricted to reach 1 at the CCD readout by replacing the data point at $y = 0$ by $\log(I) = 0$ with a small errorbar. Note that only the Mn data are used in the fit. We use the Al and Ti intensity profiles only to control the energy scaling given by eq. (2).
5. Exponent of the Chebyshev fit is used as the Y-dependence of the QEU_{BG} in each CCD column.

The fits for the 9 consecutive CCD columns (`CHIPX` $= 970 - 979$) are shown in Fig. 7. Note that the scaling of Mn fits to Ti and Al (blue and red solid lines, respectively) works fine even for very different amplitudes of the the flux loss at Mn.

4.3 Energy dependence of the BG fraction: $f_{\text{BG}}(E)$

The final ingredient of our QEU model is the energy dependence of the fraction of BG events in the total flux. We derive this ratio directly from the data using 1) ECS data at 1.5, 4.5, and 5.9 keV, 2) XRCF measurements at 0.525, 0.705, 1.740, 2.166, 6.399, and 8.040 keV, 3) calibration observation of E0102 with most photons at $E = 0.62$ and 0.94 keV, 4) observations of the cluster A1795 and SNR G21.5 near the S3 readout (bright continuum spectra in the 0.5–6 keV range). The results are shown in Fig. 8. The BG fraction in the total flux increases with energy; the data are well-fit by the relation

$$
\begin{aligned}
f_{\text{BG}}(E) &= 0.32 \times \left(1 - 0.45\,(0.5/E)^{0.5}\right) && \text{for } E < 1.837 \text{ keV} \\
f_{\text{BG}}(E) &= 0.315 \times \left(1 - 0.0225\,(E - 1.837)^{1.25}\right) && \text{for } E > 1.837 \text{ keV}
\end{aligned}
\tag{3}
$$

shown by the solid line in Fig. 8.

4.4 Bringing all pieces together

Using the QEU factorization from eq. (1) and eq. (2)–(3), we can write the QEU for the S3 chip as

$$
\text{QEU}_{\text{S3}}(X, Y, E) = 1 + 0.34 \times \left(1 - 0.5\,(0.67/E)^{0.5}\right) \times \left(\left(\text{QEU}_{\text{BG, Mn}}(X, Y)\right)^{E/5.90} - 1\right),
\tag{4}
$$

7

where $QEU_{BG, Mn}(X, Y)$ is the map with 1-column resolution derived in §4.2.

The test of the new QEU calibration is shown in Fig. 9. The residual QEU uncertainties are reduced from typical ±5% variations with the current CALDB to ±1%.

4.5 QEU for S1 chip

The derivation of QEU for the S1 chip follows a similar route with some modifications outlined below.

4.5.1 Illumination pattern

Using the spatial distribution of the GG events we verified that the S4–S2 illumination pattern is still mostly OK in S1 for the Al and Mn but not Ti lines. However, to reduce the illumination uncertainties, we flat-fielded the BG data using the GG images.

4.5.2 Serial CTI

The S1 chip appears to have a much stronger serial CTI than S3. This leads to strong intensity variations near the readout (Fig. 10) and therefore, we no longer can normalize the QEU to 1 at $Y = 0$ in each column. Instead, we normalize the QEU to 1 in the region with the highest Mn line flux, `CHIPX` $= 258 - 273$, `CHIPY` $= 16 - 112$.

4.5.3 $f_{BG}(E)$

The fraction of BG events in S1 was derived identically to that in S3 (§4.3). The data from ECS and E0102 shown in Fig. 11 is well-fit by the functional form (3):

$$
\begin{aligned}
f_{BG}(E) &= 0.21 \times \left(1 - 0.45 \, (0.5/E)^{0.5}\right) & \text{for } E < 1.837 \text{ keV} \\
f_{BG}(E) &= 0.22 \times \left(1 - 0.045 \, (E - 1.837)^{1.25}\right) & \text{for } E > 1.837 \text{ keV}
\end{aligned}
\tag{5}
$$

(solid line in Fig. 11).

4.5.4 Test

The tests of the new QEU model for S1 are shown in Fig. 12. The accuracy is worth compared to S3 (there are residual 3–5% variations), but still significantly better than with the old CALDB data.

5 QEU for FI chips

5.1 Energy dependence of QEU_{BG}

The FI chips shows a very different energy dependence of the flux in the BG event set. Projections of the observed intensities in I0 are shown in Fig. 13. Clearly, *the loss of the* BG *photons in the FI CCDs is energy-independent*,

$$
QUE_{BG,FI}(E) = \text{const.}
\tag{6}
$$

The observed profile is very flat for the GG events except for the highest `CHIPY`'s. The residuals reach 2% at `CHIPY` $= 1024$. One expects, in principle, an energy-independent trend with `CHIPY` because of the cosmic-ray induced dead-area. The CHIP-averaged dead area is $\approx 3.9\%$ (REF TO YUSAF's MEMO). It is expected that it is ≈ 1.5 smaller at the readout than at large `CHIPY`'s because the cosmic rays also hit the frame store area. The expected trend is illustrated by the dashed line in Fig. 13. There is no obvious indication for the expected trend in the data, but the discrepancy is probably within the the accuracy of the illumination pattern measurement.

5.2 Spatial dependence of $QEU_{BG}(X, Y)$

The spatial dependence of the QEU is derived using the same procedure as that for the S3 chip (§4.2). The only difference is that we use a 4-column resolution in the `CHIPX` direction because no obvious column-to-column variations are observed, and the fit uses a 2-nd order polynomial for flux instead of the 4-th order polynomial for log(flux).
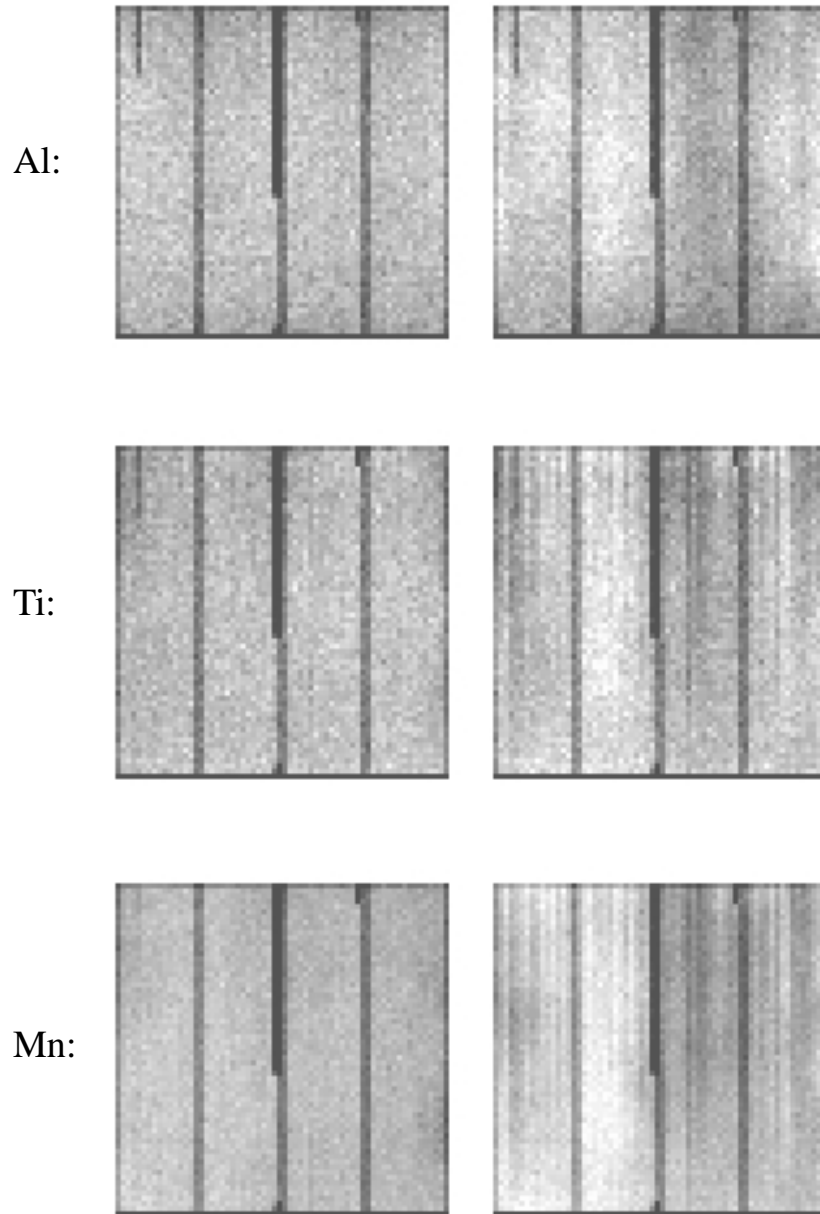
Fig. 9— Test of the new QEU model for S3. The ECS images were flat-fielded using the QEU maps described here (left) and those from CALDB (right). The full color range from black to white is 0.9–1.1 in each panel. The old QEU calibration produces ±7% residuals. The residuals are down to 1% (*rms*) and 3% (maximum) with the new model.
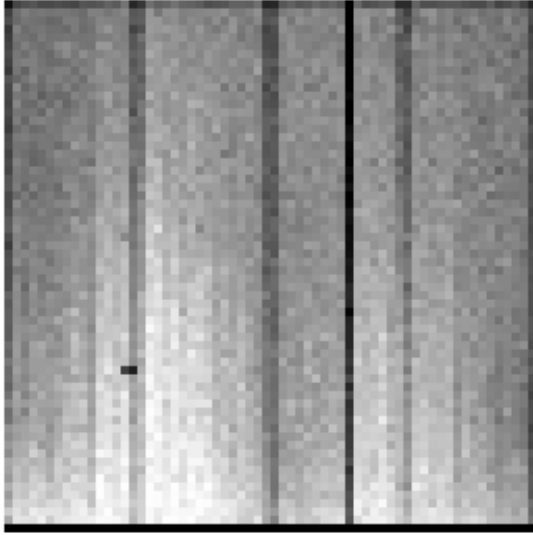
Fig. 10— Image of the S1 chip in Mn (all grades). Note strong intensity variations near the readout likely caused by the serial CTI.
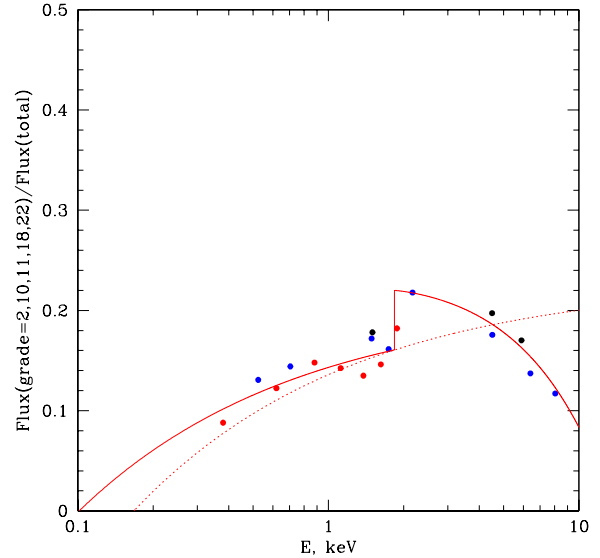

Fig. 11— The fraction of the BG events in S1 as a function of energy. The data are for ECS (black filled circles) and E0102 (red). The solid line is the fit from eq. (5) and the dotted line is from the *4/2/04* version.

5.3 Energy dependence of $f_{BG}(E)$

Since the loss of BG events is energy-independent in the FI CCDs, $f_{BG}(E)$ is the only term responsible for the dependence of QEU on energy. We derived $f_{BG}(E)$ using the ECS data, and also observations of E0102 at low energies and G21.5 at high energies. The results are shown in Fig. 14. There is a jump in the BG fraction near 1.83 keV (the Si K-edge) so it is hard to describe it by a single smooth analytic function.

Instead, we can check if this energy dependence of the BG fraction is reproduced by the ACIS simulator. The simulator results are shown by the dashed line in Fig. 14. The jump at 1.83 keV is indeed expected, and the simulator describes the data very well below this energy. Above 1.83 keV, the simulator under-predicts the BG fraction but the general trend is very close to that observed. In fact, the simulator results adjusted by a factor of 1.25 above 1.83 keV provide an excellent fit to the data (solid line). We use the adjusted simulator results as the model for $f_{BG}(E)$ in the FI CCDs.

The loss of flux in the BG events in the FI CCDs is only 10% or less (Fig. 13). Therefore, a small uncertainty in $f_{BG}(E)$ — say, 3%, — results in only a 0.3% uncertainty in the final QEU calibration. The ±0.025% band around the adapted model is shown by the dotted lines in Fig. 13. Clearly, the model accuracy is similar or better at most energies.

5.4 Test

Collecting all pieces together, the QEU in the FI chips can be written as

$$QEU_{FI}(X, Y, E) = 1 + f_{BG}(E) \times \left(QEU_{BG, Mn}(X, Y) - 1 \right) \tag{7}$$

where $f_{BG}(E)$ is from the adjusted ACIS simulator results (§5.3). The test of the new QEU in ACIS-I and the S2 chip is presented in Fig. 15.

6 Calibration data

The maps of the QEU correction for BG events is the basic ingredient of the new calibration. They have been stored in the file
/data/alexey3/chandra3/CAL/qeu_Mn_bg.fits
with a spatial resolution of 1 CCD column along CHIPX (the real resolution is 4 CCD columns for the FI chips) and 16 rows along CHIPY. NOTE: the calibration in this file is fake for the S0, S4, and S5 chips (QEU = 1).
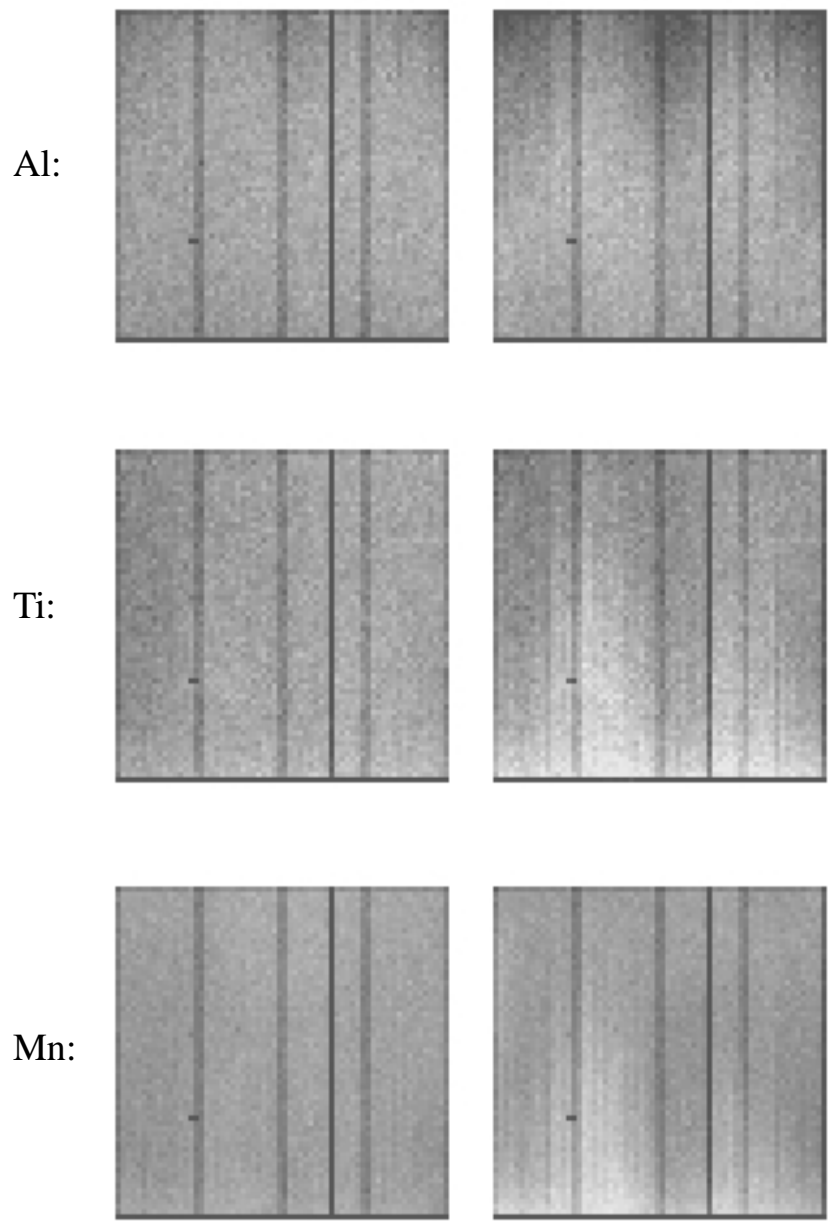
Al:

Ti:

Mn:

Fig. 12— Test of the new QEU model for S1. The new QEU model is on the left and the CALDB results are on the right. The color scale is 0.85–1.15 in each panel. The residuals are ±10% with the old calibration and ±(3 − 5)% with the new model.
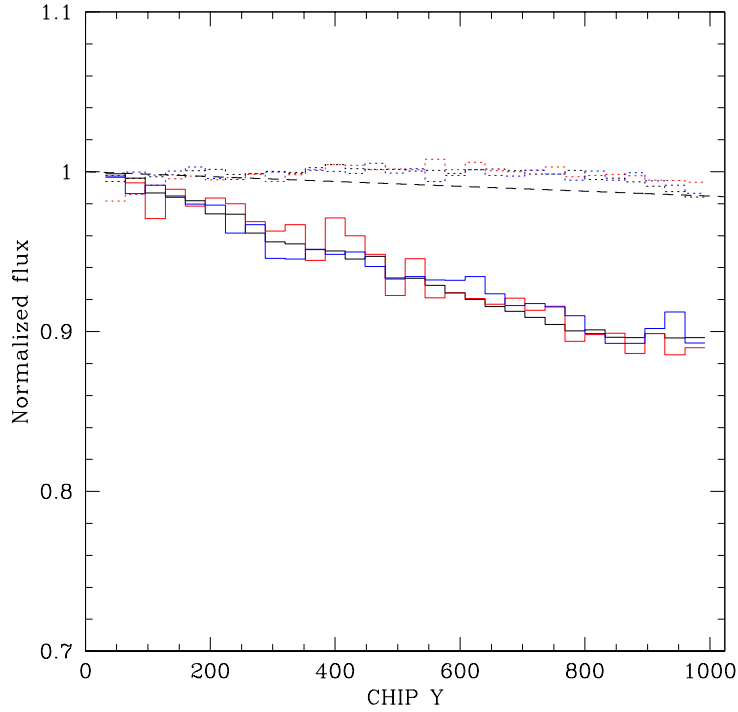
Fig. 13— Projections of the observed ECS intensity in the I0 along the CHIPX axis. The solid histograms show the data for BG events in Al, Ti, and Mn (red, blue, and black, respectively). Projections for the GG events are shown by the dotted histograms. The decrease of the Al flux at low CHIPY is consistent with the higher OBF contamination in this region. The dashed line shows the trend expected from the dead area induced by the cosmic ray events. The dashed line shows the trend expected from the dead-area effect.
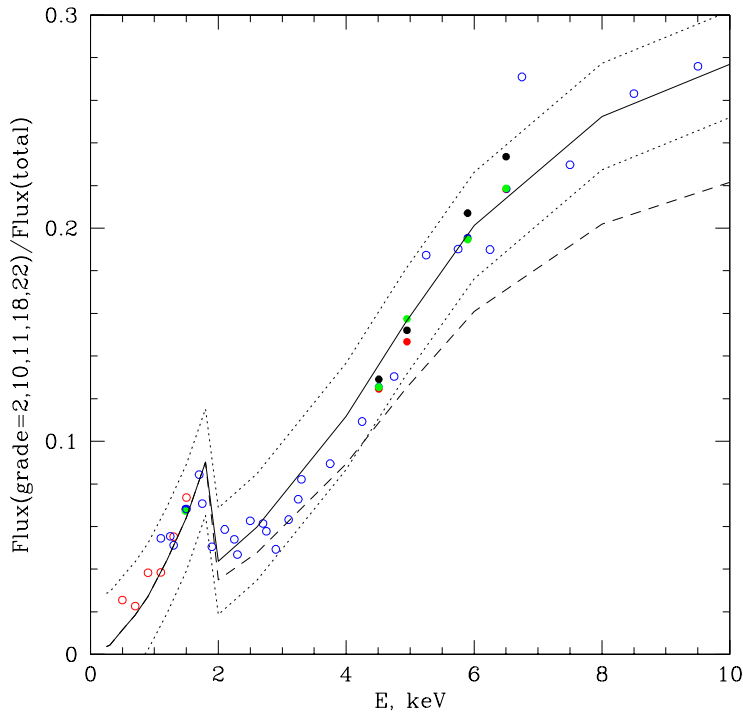

Fig. 14— Observed energy dependence of the BG fraction in the FI CCDs. The data date for the ECS lines (filled circles), G21.5 (open blue circles), and E0102 (open red circles). The dashed line is the prediction from the ACIS simulator. The solid line is the same function but scaled by a factor of 1.25 above 1.83 keV (Si-K absorption edge). The dashed lines show variations by ±2.5% around the solid line.
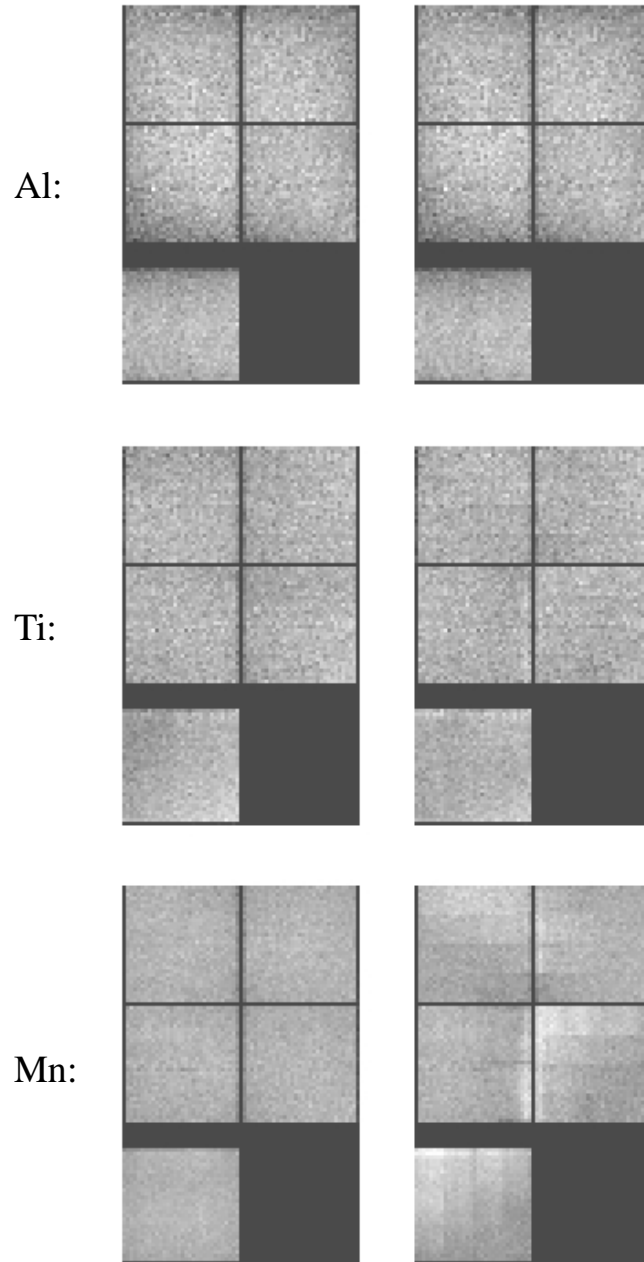
12

Fig. 15— Tests of the new QEU model in the ACIS-I and S2 CCDs. The orientation is as in the "ACIS FLIGHT FOCAL PLANE" figure (I0 is top-left, S2 is bottom-left, and I3 is middle-right) and the color scale is from 0.9 to 1.1. There is an improvement at Mn where the variations are down to ±1% (rms) or 2% (max) with the new model. The CALDB calibration produces +7%, −3% residuals in S2, and +4%, −2% in ACIS-I. The difference between the old and new models at Ti and Al are small, primarily because the corrections themselves are small. The structures visible at Al are caused by contamination on the OBF.

The final QEU can be computed using these maps and equation (4) for S3, with a slight modification (eq. (5) for S1, and equation (7) for the FI CCDs. The $f_{BG}(E)$ function for the FI CCDs is obtained by interpolation of the following table

```
  E,keV   f_BG_FI
   0.25   0.003686
   0.30   0.004381
   0.40   0.007937
   0.50   0.011565
   0.70   0.018357
   0.90   0.027143
   1.20   0.044343
   1.50   0.064109
   1.80   0.090248
   2.00   0.043669
   2.60   0.059637
   4.00   0.111774
   4.93   0.155908
   6.00   0.201254
   8.00   0.252394
  10.00   0.276859
  12.00   0.292806
```

CALCARF users can immediately access the new model by setting the following flags:

```
correct_qeu=yes
new_qeu=yes
qeuMn=$CH/CAL/qeu_Mn_bg.fits
```

For the benefit of CALDB managers, I have computed the final QEU data on a grid of energies and locations; the results can be found in the text file
`/data/alexey/ecs/QEU/CAL/qeu.txt.dat`

7 Change Log

- 4/17/04:
    1. Test of energy dependence of the BG QEU using XRCF data
    2. New energy dependence for $f_{BG}(E)$ in the BI chips.